Proceedings of the ASME 2023
International Mechanical Engineering Congress and Exposition
IMECE2023
October 29-November 2, 2022, New Orleans, Louisiana

IMECE2023- 114142

EFFECT OF INTERNAL STRUCTURE ON WARPAGE IN A LARGE-SCALE ADDITIVE MANUFACTURING PROCESS WITH BIO-DERIVED COMPOSITES

Eonyeon Jo
The Bredesen center, University of Tennessee, Knoxville

Katie Copenhaver
Manufacturing Science Division, Oak Ridge National Laboratory

Deepak Kumar Pokkalla
Manufacturing Science Division, Oak Ridge National Laboratory

Tyler Smith
Manufacturing Science Division, Oak Ridge National Laboratory

Uday Vaidya
Department of Mechanical, Aerospace, and Biomedical Engineering, University of Tennessee, Knoxville

Vlastimil Kunc
Manufacturing Science Division, Oak Ridge National Laboratory

Soydan Ozcan
Manufacturing Science Division, Oak Ridge National Laboratory

Seokpum Kim*
Manufacturing Science Division, Oak Ridge National Laboratory

ABSTRACT

Extrusion-based large-format additive manufacturing (LFAM) often results in unintended deformation and failures due to thermal residual stress between layers. This LFAM involves a hot molten polymer deposited on a previously deposited and cooled layer, generating a temperature mismatch between the layers. The temperature discrepancy causes thermal contraction mismatch, generating thermal residual stress. Due to the residual stress, printed structures experience warpage and delamination. Therefore, understanding the heat distribution behavior is essential to prevent undesired deformation and failures. The goal of this study is to investigate the effect of infill patterns on heat distribution and deformation in an LFAM system. Wood fiber-reinforced polylactic acid was used as a sustainable and low-cost reinforcement material. A numerical model was developed to predict the temperature and deformation field with thermo-mechanical properties, which were measured by a dynamic mechanical analysis and a thermal expansion test. Simulations were performed on a box geometry with three different infill patterns. The simulation model was verified with temperature data, gathered from an infrared camera. The results show a good agreement between predicted and measured temperature profiles. The developed simulation model was applied to a roof tray with different infill patterns for a case study. We found that the different thermal mass distributions resulting from the various infill patterns affected the heat distribution and deformation. These findings contribute to a better understanding of the thermal and mechanical behavior of LFAM.

Keywords: Large-format additive manufacturing, 3D printing, bio-derived composites, fiber-reinforced composites, thermo-mechanical analysis, warpage, and infill pattern.

NOMENCLATURE

δ	Density
C_p	Specific heat capacity
κ (κ_{11}, κ_{22}, κ_{33})	Thermal conductivity coefficient (in x, y, and z direction)
h_{cv}	Natural convection coefficient
ε	Emissivity
α (α_{11},α_{22},α_{33})	Thermal expansion coefficient (in x, y, and z direction)

* Corresponding author (e-mail address): Seokpum kim (kimsp@ornl.gov)

1. INTRODUCTION

Additive manufacturing (AM) has revolutionized manufacturing by providing design freedom and eliminating the need for molds or dies. The flexibility of AM processes makes them suitable for a wide range of applications in industries such as automotive, renewable energy, and aerospace manufacturing [1-3]. During AM, materials are deposited layer-by-layer to create a stable structure that must be strongly bonded to the previous layer. Depending on the process, bonding can occur through chemical reactions or melting and fusion. For example, vat photopolymerization, material jetting, binder jetting, and direct ink writing rely on chemical bonding or crosslinking of molecules, while directed energy deposition, powder bed fusion, and thermoplastic material extrusion use heat to melt and fuse new layers of material to the previous layer [4].

The recent development of extrusion-based large format AM (LFAM) processes has enabled the creation of machines with much larger build envelopes, up to 30.5 m long by 7.6 m wide by 6.1 m tall, with high deposition rates of 453 kg/hr or higher [5]. In these LFAM systems, a granular or pelletized polymer is fed into a screw-type extruder, which is similar to the feeding system used in traditional extrusion manufacturing processes [6]. The screw in the extruder generates pressure and heat to melt the feedstock, which then flows throughout the print nozzle. LFAM systems that use thermoplastic polymer deposition combine the polymer extrusion system to liquefy the feedstock with a robotic deposition system to deposit the molten substance for building a large-scale structure layer-by-layer [7]. These advances in LFAM technology have opened new possibilities to produce large, complex structures that were previously impossible to manufacture with traditional techniques. However, these structures can be susceptible to warpage due to various factors, including thermal contraction mismatch and thermal residual stress.

One of the major challenges in using such large-scale printers is the warpage and shrinkage of the deposited substance during cooling. The layer-by-layer AM deposition process results in a thermal contraction mismatch between a previously deposited cold layer and a newly deposited hot layer, which causes strain gradients between the layers [8]. These strain gradients produce shear strain within the layers, leading to the formation of thermal residual stress. Warpage is then developed as a byproduct of this thermal residual stress. Figure 1 illustrates the mechanism of warpage development between a previously printed layer and a newly deposited layer caused by the thermal contraction mismatch. As such, understanding the factors that contribute to the development of these residual stresses is critical for preventing unintended warpage and failures in LFAM processes.

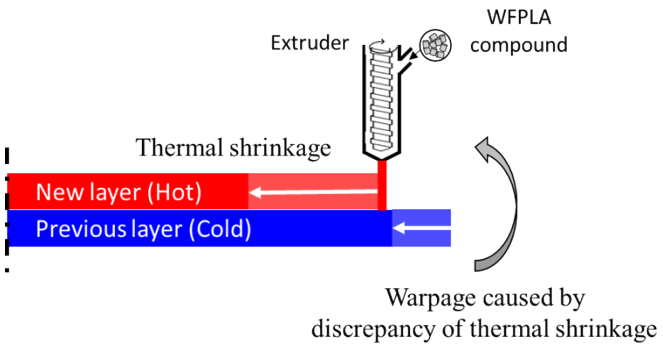

Figure 1: Schematic of warpage caused by difference of thermal shrinkage between a previously cooled layer and a newly extruded hot layer.

The infill pattern, also known as the raster pattern, fills the inside area of the printed structure. The infill density directly affects the tensile properties, dynamic storage modulus, inversely proportional loss modulus, and damping factor of the structure [9]. Additionally, the temperature distribution of AM structures can be controlled by a combination of the raster pattern and material design [10]. Thermal mass concentration also can be changed by the infill pattern. This effect is more significant in LFAM processes due to the larger amount of deposition substance, which generates a lot of residual heat. Therefore, understanding the role of infill patterns in the formation of thermal residual stress and warpage is crucial for optimizing the quality and properties of LFAM structures.

The present work focuses on investigating the effect of infill patterns on warpage in an LFAM process. To achieve this, we printed simple box geometry structures with different infill patterns. A finite element analysis (FEA) model was designed to predict temperature history and deformation for the AM process. The simulation model was verified through experimental results. Using the developed FEA model, we predicted the temperature profiles and deformation of a roof tray to examine the effect of infill patterns on the roof tray's warpage. By analyzing the results, we aim to provide insights into the role of infill patterns in mitigating the warpage in LFAM processes.

2. MATERIALS AND EXPERIMENTS

Thermally modified wood fiber reinforcement was compounded with polylactic acid (PLA). The thermoplastic compound was used as an extruded material in an LFAM system. The mechanical properties (tensile and DMA) and thermal properties (CTE) have been evaluated for the additively manufactured specimens with the wood fiber-reinforced polylactic acid (WFPLA).

2.1 Material characterization

Tensile testing was conducted on additively manufactured specimens with PLA filled with 20wt% wood fiber from the big area additive manufacturing system (BAAM) system at Oak Ridge National Laboratory (ORNL). Specimens were cut into

the dog bone shape in the printing direction (x-direction) and stacking direction (z-direction) to determine anisotropic mechanical properties.

The gauge width of the specimens was 13 mm, and the thicknesses were 7 mm. Each specimen was tested at a rate of 5 mm/min and an extensometer was used to collect strain data. By analyzing the stress-strain curves for each specimen from tensile testing, the elastic modulus, ultimate tensile strength (UTS), and strain to failure were characterized. The results are summarized in Table 1. The WFPLA showed highly anisotropic by the modulus, strength, and strain to failure being high in the printing direction (x-direction), due to the fiber direction, which is aligned with the direction of printing, and lower strength in the z-direction with lower inter-bead adhesion compared to intra-bead adhesion.

Table 1: Mechanical testing results of the additively manufactured specimens with WFPLA.

Printing direction	Modulus (GPa)	UTS (MPa)	Strain to failure (%)
x-direction	4.87 ± 0.15	44.02 ± 2.49	2.34 ± 0.8
z-direction	3.81 ± 0.12	24.75 ± 0.8	0.953 ± 0.09

Dynamic mechanical analysis (DMA) was conducted on additively manufactured WFPLA specimens in both the x and z directions. The width of the specimens was 10mm, and the thickness was 3mm. Each specimen was tested using a three-point bend clamp with a span of 35mm. The oscillatory displacement was $\pm\ 15\mu m$ and the temperature was ramped from 30°C to 120°C at a rate of 3°C/min.

Thermal expansion testing was conducted on additively manufactured WFPLA. The testing utilized a digital image correlation (DIC) technique. For the DIC measurements, a block of material was printed and machined into a cube shape. The sample block was printed with a simple raster pattern. The machined cube had a size of 101.6 x 101.6 x 101.6mm. The cube was speckled with spots of ink for coordinate tracing during the DIC process. The details of the DIC technique for large-scale 3D printed material are described in Ref. [11].

2.2. Large-scale AM printing

Three boxes were printed using WFPLA to observe how different infill patterns affect the cooling and warpage in the LFAM print. The first box was printed with concentric squares, beginning at the outer edge, and going inwards. In the box print, the largest square was printed first, and smaller squares were printed inside the previous bigger one ("outside-in"). The second box employed the same concentric square printing procedure as the first box printing, but this time the smallest inner square was printed first, followed by larger squares ("inside-out"). A simple raster infill pattern was used to print the final box. To unify the production environment, the three boxes were printed simultaneously, sharing the same layer deposition time. An infrared (IR) camera was used to gather a series of thermal images during the whole print procedure, and the IR thermal image in greyscale can be seen in Figure 2. In the process, the deposition temperature was 210 °C and the base was heated up to 50°C, and the printed boxes with different infill patterns are shown in Figure 3.

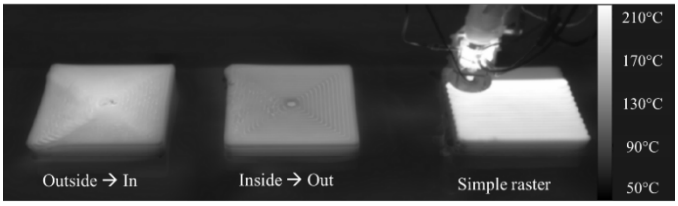

Figure 2: IR thermal image in greyscale during the LFAM printing. Three boxes with different infill patterns were simultaneously fabricated to share the same layer deposition time.

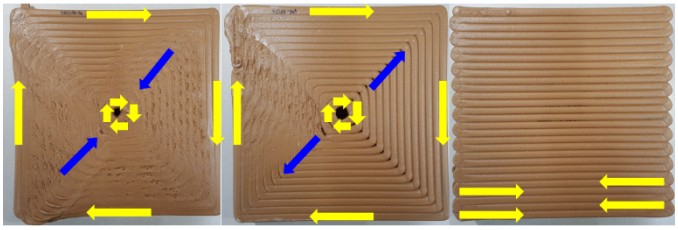

Figure 3: Box prints with varying infill patterns (a) concentric square box from outside to in, (b) concentric square box from inside to out, and (c) simple raster.

3. NUMERICAL SIMULATION

A numerical simulation model for the AM process was developed to predict the temperature profiles and deformation, based on finite element analysis. In the numerical model, heat transfer occurs by thermal conduction, convection, and radiation. The WFPLA material considered in this study exhibits anisotropic thermal properties due to the presence of the reinforced wood fibers. The addition of fiber reinforcements may increase the thermal conductivity of the composite along the fiber direction [12]. Therefore, fiber orientation plays a crucial role in predicting temperature profiles and layer temperatures. Considering that the reinforced fiber in the extruded substance is aligned with the tool path direction, the principal direction (x-direction) for fibers is chosen as the print direction and the z-direction is chosen as the stacking direction.

In the AM process simulations, progressive material activation was used to simulate the additive manufacturing process. The tool paths used in the LFAM system were converted as simulation codes with a developed tool path converter. The converter changed Gcode into an event series composed of time, deposition position, and extruder on-off information. To implement the layer-by-layer deposition, the elements were generated vertically with the stacking direction, and the height of a mesh was made in the portion of the height of a layer. When the tool path passed through the element, the element was activated, and the boundary conditions continuously were updated over the entire simulation.

The AM process simulation model utilized a sequentially coupled thermomechanical simulation technique, consisting of two steps: transient heat transfer analysis and structural analysis. In the first step, the temperature data during the cooling process was obtained through a transient heat transfer analysis using a heat transfer element (mesh type=DC3D8). The three-dimensional anisotropic thermal conductivity was governed by three conductivity parameters ($\kappa_{11}, \kappa_{22}, \kappa_{33}$) for the x, y, and z directions, with the principal direction (x-direction) chosen as the deposition direction and the z-direction chosen as the stacking direction due to the alignment of reinforced fibers along the tool path direction. Newton's law of cooling with a constant convection coefficient (h_{cv}) was used for natural convection. The convection coefficient was calibrated by comparing the cooling behavior of the printed substance between the experiment and the simulation. Thermal radiation was governed by the Stefan-Boltzmann law with a constant emissivity (ε). The material properties used for the analysis were summarized in Table 2. In the second step, structural analysis was conducted, based on the previously obtained temperature data, to predict deformation with the structural element (mesh type=C3D8). The boundary conditions for the thermomechanical analysis are shown in Figure 4.

Table 2: Material properties for numerical simulations.

Variable name	Unit	Value
δ	kg/m^3	1240
C_p	$J/(kg \cdot K)$	1476
$\kappa_{11}, \kappa_{22}, \kappa_{33}$	$W/(m \cdot K)$	0.19, 0.18, 0.16
h_{cv}	$W/(m^2 \cdot K)$	1
ε	-	0.85
$\alpha_{11}, \alpha_{22}, \alpha_{33}$	$10^{-6}/°C$	67.7, 94.0, 112.2

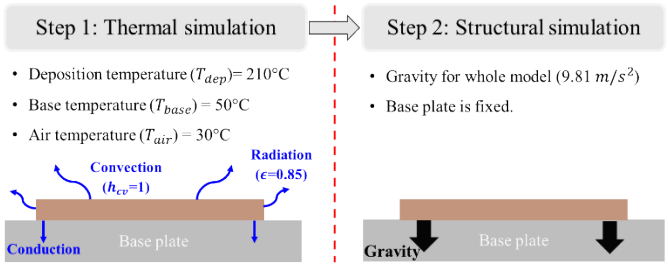

Figure 4: Boundary conditions for sequentially coupled thermomechanical simulation model.

3.1 Simulation model for box print

An FEA simulation model for the box print was designed to predict the temperature profiles and the warpage with the different infill patterns. The G-code used in the experiments was converted into an event series for the element activation technique. To implement layer-by-layer deposition, elements were generated vertically with the stacking direction, and the mesh height was kept the same as the printed layer height. The printed boxes had 10 layers in total, and the mesh had also 10 layers. Figure 5 shows the geometry of the box and the FEA mesh used in the simulation. The layer deposition times for all cases were the same, regardless of infill patterns since they were simultaneously fabricated. The overall printing time was 3907 seconds.

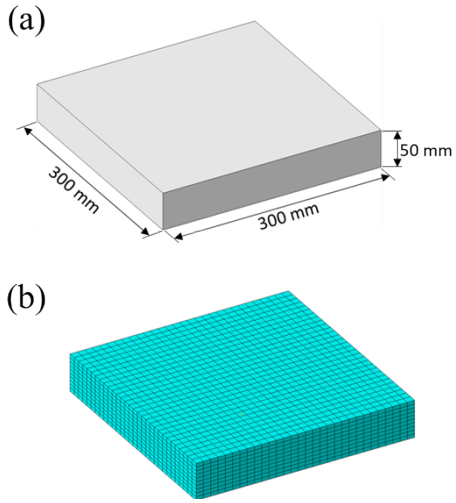

Figure 5: (a) CAD geometry of the box prints and (b) finite element of mesh of the box.

3.2 Simulation model for roof tray

To apply our simulation model to a practical case, we designed a roof tray for BAAM printing. The design is based on a roof tray available in the market and was modified to include three different infill patterns. The roof tray's size was approximately 1.5m long by 1m wide, and its design is shown in Figure 6(b), with the original roof tray design shown in Figure 6(a).

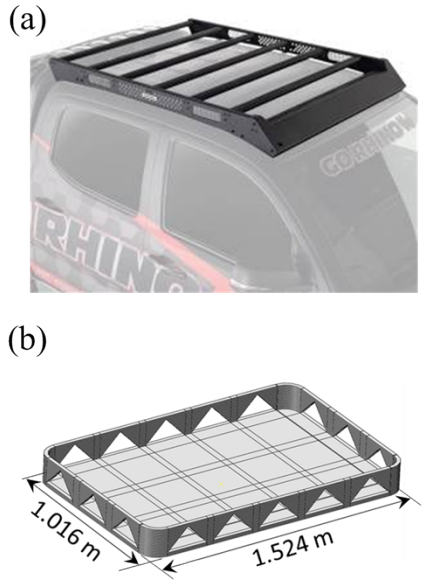

Figure 6: (a) Roof tray in the market (image from https://www.gorhino.com) and (b) Roof tray designed for BAAM printing.

We considered three different infill patterns for the roof tray, as shown in Figure 7. The first infill pattern, shown in Figure 7(a), was a concentric fill from the outside boundary toward the inside. The second infill pattern, shown in Figure 7(b), was a concentric fill from the inside toward the outside boundary. Finally, the third infill pattern, shown in Figure 7(c), was a simple raster infill pattern. By simulating the printing process of the roof tray with each of their infill patterns, we were able to investigate their impact on heat distribution and deformation in the printed structure.

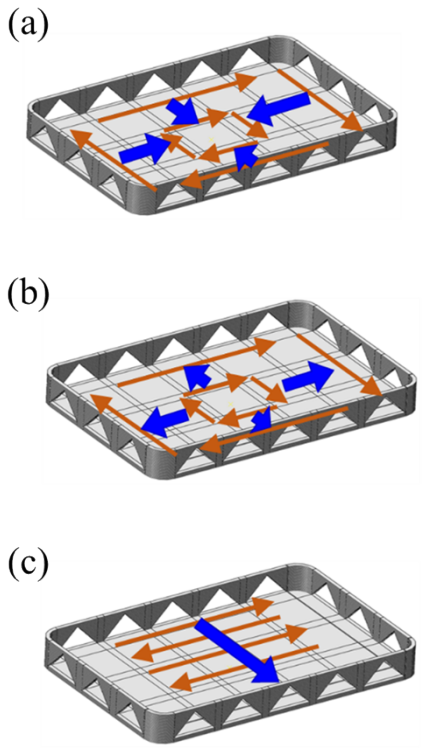

Figure 7: Three different infill patterns: (a) Concentric (following the boundary lines) from outside toward inside, (b) Concentric (following the boundary lines) from inside toward outside, (c) Simple raster.

4. RESULTS AND DISCUSSION

4.1 Simulation results for the box print

The FEA simulation comprises two coupled steps to predict both the temperature field and the deformation. Firstly, a heat transfer analysis was conducted to predict the temperature field for the box prints with different infill patterns. The heat transfer simulation considers thermal conduction, convection, and radiation as the mechanisms for heat transfer. The ambient temperature and the base temperature were set as boundary conditions. A comparison of temperature fields in experiments and simulations when the last layer was deposited is shown in Figure 8. The temperature range is 50°C (base temperature) to 210°C (extrusion temperature), and the red area means the higher temperature region. The tool path can be inferred by tracking the temperature field since the newly extruded material has a high temperature.

Moreover, comparisons of temperature profiles between experimental measurements from an infrared camera and simulation predictions were conducted for the y-directional position at the center of the boxes and the results are shown in Figure 9. In the figure, the blue lines represent the experimental results, and the red lines show the simulation results. The simulation results show a good agreement with the experimental results for all cases, which confirms the reliability of the conducted simulations in predicting the temperature field.

In the second step of our simulation model, we aimed to predict the warpage deformation of the box prints by conducting a structural analysis based on the temperature data obtained from the heat transfer analysis. As the temperature change in the prints causes thermal residual stress generated by the thermal contraction of the material, it is crucial to conduct a structural analysis in coupling with the time-dependent temperature change to predict the deformation accurately. The displacement fields in the layer stacking direction for the box prints were then analyzed and visualized in Figure 10, providing insights into the deformation behavior of the prints with different infill patterns.

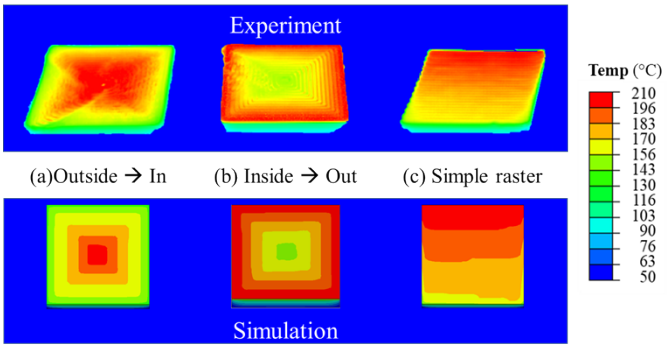

Figure 8: Comparison of temperature field measured experimentally and predicted with simulation with different toolpath at the last of the printing process (last layer deposition).

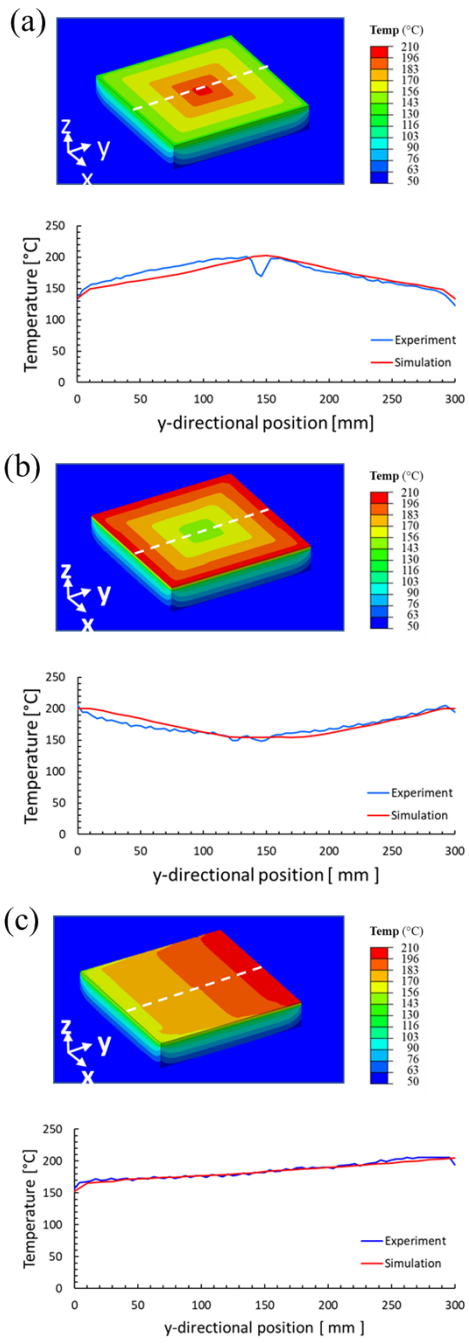

Figure 9: Comparison of temperature profile across the y-directional position measured experimentally and predicted with simulation at the last of the printing process (last layer deposition), (a) concentric square box from outside to inside, (b) concentric square box from inside to outside and (c) simple raster.

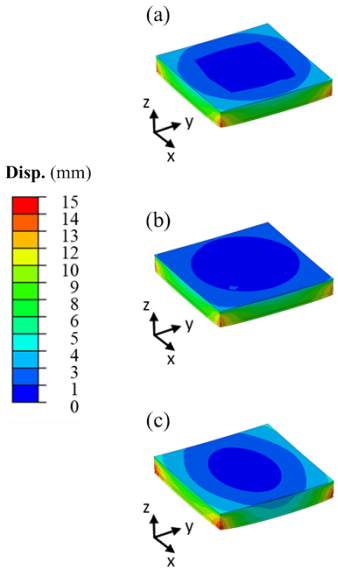

Figure 10: Displacement filed in the layer stacking direction (z-direction), (a) concentric square box from outside to inside, (b) concentric square box from inside to outside, and (c) simple raster.

4.2 Simulation results for the roof tray

As shown in Figure 11 and Figure 12, temperature fields and the corresponding deformation fields have been obtained from the simulation. The temperature field of the concentric print from the outside to the inside shows a higher temperature at the center, while the temperature field of the concentric print from the inside to the outside shows a higher temperature at the periphery. The temperature field of the print with a simple raster line shows a gradual decrease.

We observed that the temperature field from the raster line infill pattern had the least amount of non-uniformity in temperature difference within the domain. As a result, it yielded the least amount of deformation compared to the other infill patterns. Specifically, we found that the raster line infill pattern showed a lower temperature and a more uniform temperature distribution, resulting in less thermal residual stress and reduced deformation in the printed structure.

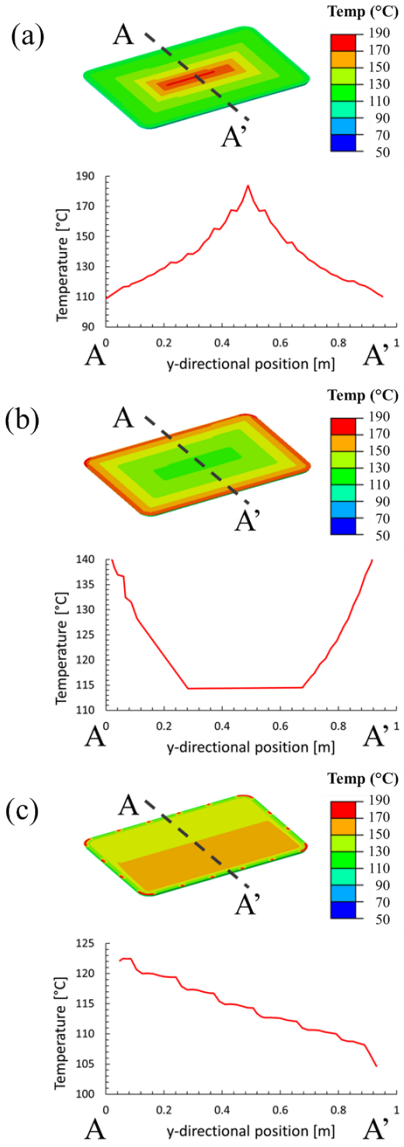

Figure 11: Comparison of temperature filed with three different infill patterns: (a) concentric from outside toward inside, (b) concentric from inside toward outside, and (c) simple raster.

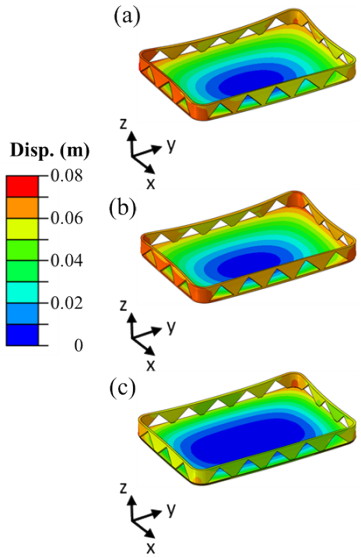

Figure 12: Comparison of deformation filed with three different infill patterns: (a) concentric from outside toward inside, (b) concentric from inside toward outside, and (c) simple raster.

5. CONCLUSION

In this study, we have investigated the effect of infill patterns on heat distribution and deformation in an extrusion-based large format additive manufacturing system. Through a combination of experiments and numerical simulations, we have demonstrated that different infill patterns can have a significant impact on the thermal behavior of printed structures, ultimately affecting their warpage. Our experiments and simulations have shown that a simple raster infill pattern can result in the least amount of thermal residual stress and deformation, making it an attractive option for large format additive manufacturing applications. We have developed a numerical simulation model to predict the temperature distribution and deformation of a roof tray design with different infill patterns. Overall, our study has highlighted the importance of considering infill patterns in large format additive manufacturing processes. By optimizing these design parameters, it may be possible to mitigate unintended deformation. Future work in this area could explore the use of more complex infill patterns and lattice structures, as well as the integration of other process parameters such as printing speed and temperature control.

ACKNOWLEDGEMENTS

This research is sponsored by the U.S. Department of Energy, Office of Energy Efficiency and Renewable Energy, Industrial Technologies Program, under contract DE-AC05-00OR22725 with UT-Battelle, LLC.

REFERENCES

[1] A. A. Shapiro, et al., "Additive Manufacturing for Aerospace Flight Applications," *Journal of Spacecraft and Rockets,* vol. 53, no. 5, 2016.

[2] M. Talagani, et al., "Numerical Simulation of Big Area Additive Manufacturing (3D Printing) of a Full-Size Car," *Sampe Journal*, vol. 51, no. 4, pp. 27-36, 2015.

[3] S. L. Marasso et al., "PLA conductive filament for 3D printed smart sensing applications," *Rapid Prototyping Journal*, vol. 24, no. 4, pp. 739-743, 2018.

[4] Standard Terminology for Additive manufacturing Technologies, *ASTM Standard F2792-12a*, International, 2012, 10.1520/F2792-12.

[5] B. K. Post, et al., "Big Area Additive Manufacturing Applications in Wind Turbine Molds," *Solid Freeform Fabrication an Additive Manufacturing conference*, 2017.

[6] A. Bellini, et al. "New developments in fused deposition modeling of ceramics," *Rapid Prototyping Journal*, vol. 11, pp. 214–220, 2005.

[7] C. E. Duty, et al., "Structure and mechanical behavior of big area additive manufacturing (BAAM) materials," *Rapid Prototyping Journal*, vol. 23, pp. 181–189, 2017.

[8] B.G. Compton, et al., "Thermal analysis of additive manufacturing of large-scale thermoplastic polymer composites," *Additive Manufacturing*, vol. 17, pp. 77–86, 2017.

[9] Y.Y. Aw, et al., "Effect of printing parameters on tensile, dynamic mechanical, and thermoelectric properties of FDM 3D printed CABS/ZnO composites," *Materials*, vol. 11, no. 4, 2018.

[10] C. Shemelya, et al., "Anisotropy of thermal conductivity in 3D printed polymer matrix composites for space-based cube satellites," *Additive Manufacturing*, vol. 16, pp. 186–196, 2017.

[11] D. Hoskins, et al., "Modeling thermal expansion of a large area extrusion deposition additively manufactured parts using a non-homogenized approach," *Solid Freeform Fabrication*, pp. 1165–1174, 2019.

[12] L.J. Love, et al., "The importance of carbon fiber to polymer additive manufacturing," *Journal of Materials Research,* vol. 29, no. 15, pp. 1893–1898, 2014.